

Structural Determinants of Sequence Evolution in Enzymatic proteins

AMIR SHAHMORADI¹, CLAUS O. WILKE²

¹ *Department of Physics, The University of Texas at Austin, TX 78712, USA; amir@physics.utexas.edu*

² *Department of Integrative Biology, The University of Texas at Austin, TX 78712, USA;
wilke@austin.utexas.edu*

What are the best structural predictors of protein's sequence evolution? A number of site-specific structural properties have been proposed over the past decade to answer this question. The majority of these quantities however, depend on the set of atomic coordinates used to represent individual sites in proteins, and often involve one or more number of adjustable parameters in their definition. A number of studies have already demonstrated that the choice of C_α atomic coordinates may not be an optimal representation of the protein's 3-dimensional structure, in particular for the calculation of site-specific quantities such as Weighted Contact Number. Expanding on these studies, here we propose a new set of parameter-free structural variables derived from the Voronoi tessellation of protein structure which perform equally well or better than virtually all previously-considered structural quantities in predicting protein sequence evolution. We further show that the ideal representation of the 3-dimensional structure of proteins is the set of geometric average coordinates of atoms in the side chains of individual amino acids versus the common choice of backbone C_α coordinates. Long-range interactions between individual amino acids are found to have a minor but significant contribution to the evolutionary patterns of protein sequence.

1 Introduction

A variety of site-specific structural characteristics have been proposed over the past decade to predict protein sequence evolution from structural properties. Among the most important and widely discussed are the Relative Solvent Accessibility (RSA) (e.g., Goldman et al., 1998; Bustamante et al., 2000; Conant and Stadler, 2009; Franzosa and Xia, 2009; Ramsey et al., 2011; Scherrer et al., 2012; Meyer and Wilke, 2013; Meyer et al., 2013; Yeh et al., 2014a,b; Shahmoradi et al., 2014; Sikosek and Chan, 2014; Meyer and Wilke, 2015), Contact Number (e.g., Rodionov and Blundell, 1998; Hamelryck, 2005; Liao et al., 2005; Bloom et al., 2006; Huang et al., 2014; Marcos and Echave, 2014; Yeh et al., 2014b,a; Shahmoradi et al., 2014; Meyer and Wilke, 2015), measures of thermodynamic stability changes due to mutations at individual sites in proteins (e.g., Wilke et al., 2005; Echave et al., 2014), and measures of local flexibility, such as the Debye-Waller factor (hereafter B factor) (e.g., Liao et al., 2005; Shih et al., 2012; Shahmoradi et al., 2014) or flexibility measures based elastic network models (e.g., Liu and Bahar, 2012) and Molecular Dynamics (MD) simulations (e.g., Shahmoradi et al., 2014).

Although structural characteristics have been individually extensively studied and explored with regards to their association with sequence evolution, it is yet unknown whether these seemingly independent quantities are merely different manifestations of a more fundamental underlying characteristics of individual sites in proteins or each influence the sequence evolution independently. It is perceivable that quantities such as B factor, RSA, and CN, all serve as a proxy measures of local packing density of individual sites in proteins, or the local flexibility of individual amino acids. Franzosa and Xia (2009) use a variety of structural variables representing the local packing density to show that RSA is the key determinant of sequence evolution with packing density having only peripheral influence. Recently however, Huang et al. (2014) have argued, through an extensive mathematical formulation within the framework of Elastic Network Models, for the local packing density as the dominant factor in sequence variability patterns in contrast to RSA and local flexibility measures.

It is notable that the site-specific flexibility is often represented by C_α atomic B factor, a quantity that is not necessarily an unbiased measure of the amino acid flexibility as a whole in a given site in protein. A more accurate measure of amino acid flexibility requires the calculation of accessible free volume to each site in protein structure. An estimate of the accessible volume for each site in protein can be generally obtained through a quantity widely known as Contact Number introduced and discussed by several authors (e.g., Liao et al., 2005). In its simplest mathematical form, the Contact Number for a given site in protein is defined as the number of amino acids within a fixed radius r of neighborhood around it (e.g., Franzosa and Xia, 2009). Individual sites are generally represented by the coordinates of C_α backbone atoms for the calculation of CN. A major problem with the traditional definition of contact number however, is the existence of the arbitrary parameter r in the definition of CN. There is no consensus on the optimal value of this cutoff distance, although it is typically chosen in the range 7 Å to 13 Å (e.g., Lin et al., 2008; Franzosa and Xia, 2009).

In an attempt to provide a more general definition of CN, some studies (e.g., Lin et al., 2008) have already suggested an alternative definition known as the Weighted Contact Number (WCN): For a given site i in a protein of length N , WCN_i is defined as the sum of the inverse-squared of distances between the amino acid of interest and all other sites in protein,

$$WCN_i = \sum_{j \neq i}^N \frac{1}{r_{ij}^2}, \quad (1)$$

Although WCN is in general a better predictor of C_α atomic B factor and site-specific sequence variability, the proposed definition of WCN still involves an adjustable free parameter, the exponent of the power-law kernel, which is typically fixed to $\alpha = -2$ as shown in Eqn 1 (e.g., Yang et al., 2009). More-

over, no physical model has been so far proposed to support the power-law kernel used in the definition of WCN and the specific value of exponent often used.

Motivated by the existing gaps in the current understanding of the role of flexibility and other structural properties on sequence-structure relations in proteins, here we propose and derive a new set of site-specific structural properties which, unlike CN and WCN, their definitions does not involve any free parameters, while performing equally well or better than all previously-considered structural quantities in predicting protein sequence evolution. This is done by employing tessellation methods from the field of computational geometry to calculate several new characteristics of sites in proteins, which can serve as proxy measures of local packing density and site-specific flexibility. Contrary to what is currently perceived about the role of flexibility in sequence variability (e.g., Huang et al., 2014), we show that the newly calculated flexibility measures outperform many of previously studied structural properties, such as RSA and the traditional definitions of Contact Number (CN) and the Weighted Contact Number (WCN), in predicting sequence evolution at residue level.

Furthermore, for structural properties that are calculated based on a set of representative site coordinates, we show that the choice of the geometric average of the side chain atomic coordinates instead of the traditional choice of C_α atomic coordinates, always results in significantly better predictions of site-specific sequence evolution. Similar improvements in correlations with different site-specific structural properties and sequence variability measures are also observed if the average of side chain B factors, instead of C_α atomic B factor, is used as a proxy measure of site flexibility.

2 Protein Dataset and Structure/Sequence Variability Measures

The entire analyses and results presented in this work are based on a dataset of 209 monomeric enzymes (e.g., Yeh et al., 2014b; Echave et al., 2014) randomly picked from the Catalytic Site Atlas 2.2.11 (Porter et al., 2004) with protein sizes in the sample ranging from 95 to 1287 amino acids, including representatives from all six main EC functional classes (Webb, 1992) and domains of all main SCOP structural classes (Murzin et al., 1995). To assess the evolutionary rates at the amino acid level for each protein, first a set of up to 300 homologous sequences were collected by Yeh et al. (2014b) for each protein from the *Clean Uniprot* database following the ConSurf protocol (Goldenberg et al., 2009; Ashkenazy et al., 2010). Sequence alignments were then constructed using amino-acid sequences with MAFFT (Katoh et al., 2005), specifying the auto flag to select the optimal algorithm for the given data set, and then back-translated to a codon alignment using the original nucleotide sequence data. The alignments were then used to calculate the site-specific sequence variability for each individual protein in dataset. For each structure, the respective sequence alignment and phylogenetic tree were used to infer site-specific substitution rates with Rate4Site, using the empirical Bayesian method and the amino-acid Jukes-Cantor mutational model (Mayrose et al., 2004), hereafter abbreviated as *r4sJC*.

In addition site-specific evolutionary rates, we also calculated the Shannon entropy (H_i) – the sequence entropy (Shenkin et al., 1991) – at each alignment column i , based on the assumption that the occurrence of each of the 20 amino acids is equally likely at any given site in the alignments:

$$H_i = - \sum_j P_{ij} \ln P_{ij} \quad (2)$$

where P_{ij} is the relative frequency of amino acid j at position i in the alignment. We use DSSP software (Kabsch and Sander, 1983) for the calculation of the Accessible Surface Area (ASA) for each site normalized by the theoretical maximum solvent accessibility values of Tien et al. (2013) to obtain the Relative Solvent Accessibility (RSA) for all individual sites in all proteins. The *ddG rate* estimates for all

structures in the dataset were calculated using FoldX program (c.f., Echave et al., 2014, for details of the methodology employed). In brief, the site-specific quantity, ddG rate, is a proxy measure of the stability of the entire structure of protein upon substituting an amino acid in a given site with all other 19 amino acids. Therefore, a low ddG rate for a given site would indicate a high chance of structure perturbation upon substitution and therefore high conservation of the specific amino acid in the site on evolutionary timescales.

A measure of thermodynamic stability changes due to amino acid substitutions at individual sites in proteins can be defined and obtained following the stability threshold model of Bloom et al. (2006) Bloom et al. (2006), which was also recently further studied by Echave et al. (2014) Echave et al. (2014). Based upon this model which was extensively described in Chapter ??, a quantity $\Delta\Delta G$ rate (or it ddG rate) was derived for each individual site in all proteins in dataset. A high ddG rate for the i^{th} site in a protein indicates a high stability of the site and the overall conformation of the protein to perturbations caused by substitution of the amino acid residing the site.

As a measure of local flexibility or fluctuation in different parts of the protein structure the temperature, factors (*B factor*) for all atoms in PDB files were extracted (c.f., Chapter ??). Although, B factor is an atomic measure of flexibility and fluctuation in proteins, the backbone C_α B factor has become a very popular proxy measure of amino acid flexibility in the studies of protein dynamics and benchmarking of different Elastic Network Models of proteins. Alternatively, the site-specific fluctuation could be calculated from MD simulations. This was however impossible for this study for the large dataset of 209 proteins considered in this work.

All data including a list of 209 proteins and their properties together with Python, R and Fortran codes written for data reduction and analysis are publicly available to view and download at <https://github.com/shahmoradi/cordiv>.

3 Results

Voronoi Partitioning of Protein’s Structure

There is already extensive body of literature on the applications of different methods of structural partitioning in the studies of protein structure and its prediction from sequence Richards (1974); Gerstein et al. (1994). The Voronoi tessellation and its dual graph, the Delaunay triangulation, have particularly attracted much attention in the studies of protein internal structure and development of empirical potentials Zomorodian et al. (2006); Zhou and Yan (2014); Xia et al. (2014). For a given a set of centroid points (seeds) in 3-dimensional Euclidean space, the simplest and most familiar case of Voronoi tessellation divides the space into regions, called *cells*, such that the cell for each centroid point consists of every region in space whose distance is less than or equal to its distance to any other centroid points (Figure 1).

In the context of protein studies, the atomic coordinates of C_α backbone atoms have been widely used as the set of Voronoi seeds to partition the 3D structure of protein according to Voronoi tessellation. An example of Voronoi tessellation of protein structure in two dimensions (PDB ID: *1LBA*) is shown in Figure 1. The properties of individual cells resulting from tessellation are then used to obtain a wide range of information on protein structure, energy landscape or protein–protein interactions.

Here in this work, the simplest and most widely used definition of Voronoi tessellation described above is applied on a dataset of 209 monomeric enzymes. We use VORO++ software Rycroft (2009) to calculate the relevant Voronoi cell properties of all sites in all proteins in the dataset. Among the most important properties are the length of the cell edges, cell area and volume, number of faces of each cell,

the cell eccentricity defined as the distance between the cell’s seed and the geometrical center of the cell. A measure of the cell *eccentricity* can be also obtained by finding the distance between the cell seed and geometrical center of the cell. In addition, the cell *sphericity* can be calculated as a measure of the cell’s *compactness* defined as,

$$\Psi = \frac{\pi^{\frac{1}{3}}(6V)^{\frac{2}{3}}}{A}. \quad (3)$$

in which V & A stand for the volume & area of the cell respectively. For a perfectly spherical cell, $\Psi = 1$, while it becomes zero for a 2-dimensional object that has no volume but only surface area.

Voronoi Cell Area and Volume as Proxy Measures of Local Packing Density and Flexibility in Proteins

In order to assess the prediction power of site-specific variables derived from Voronoi tessellation, first the geometric centers of all side-chains for each of the proteins in dataset were calculated and used as the seeds of Voronoi polyhedra. Figure 2 depicts the distributions of the Spearman’s correlation coefficients of five most important Voronoi cell characteristics with site-specific evolutionary rates (ER). It is notable that all cell characteristics in the plot correlate positively with ER, except the cell sphericity which is always negatively correlated with ER and other Voronoi cell properties. In general, it is observed that the cell surface area has the best prediction power compared to other cell characteristics, followed by the cell volume, cell eccentricity as defined in previous section, cell’s total edge length, and the cell sphericity.

The cell properties are also strongly correlated with each other. Although the Voronoi cell volume is the second best correlating variable with ER, it exhibits no significant independent correlation with ER once we control for the cell area, with the median of its distribution centered at ~ 0.0 , as illustrated in Figure 3. Conversely, the cell sphericity and eccentricity both exhibit median partial correlations of ~ -0.1 & ~ 0.07 with ER respectively, when the contribution from the Voronoi cell area is controlled. In conclusion, the cell area, volume, and edge length appear to almost represent the same property of the Voronoi cell. Other Voronoi cell characteristics, such as the number of vertices, faces and edges of the cell also tend to correlate weakly with sequence evolutionary rates. These cell characteristics are however, discrete (integer) quantities and in general have a limited range.

Not shown here for brevity, almost identical results to the above are obtained if sequence entropy as defined by Eqn. 2 were used in place of sequence evolutionary rates. The use of sequence entropy however, generally results in weaker correlation strengths due to the discreteness and limited range inherent in the definition of sequence entropy.

One potential caveat with Voronoi tessellation of finite structures in Euclidean space is the *edge effects*. Sites that are close to the surface of protein are often associated with Voronoi cells that are bounded by the cubic box containing the protein (Figure 1). Here to ensure that these edge effects do not influence the observed sequence-structure correlations, the open cells – i.e., cells that are partially bounded and closed by the cubic box containing the protein – are identified in all proteins by examining the variations in individual cell volumes upon changing the size of the cubic box containing the protein to a given extreme value. The open cells in individual proteins are then ranked by the fraction of volume changes observed upon changing the box size and then normalized to the the largest volume observed among closed cells. It should be noted that the specific extreme value chosen for the box sizes of the proteins or the rank ordering of the open cells does not have any influence on the resulting correlation strengths, since the Spearman’s ρ by its definition is a rank correlation coefficient.

Our conclusion is that the *edge effects* due to Voronoi tessellation appear to have $\lesssim 0.01$ influence on the observed sequence-structure correlations in the dataset of 209 proteins considered in this work.

Similar conclusions are reached if the open cells were alternatively ranked by different criteria such as the fractional changes in cell area (vs. cell volume) upon changing the box size. The Voronoi cell characteristics, in particular cell volume and cell area can be safely used in predicting sequence variability without recourse to corrections for edge effects. An exception however is cell sphericity as defined in Eqn. 3, which turns out to behave differently for open and closed cells. This is well illustrated in the adjacent averaging plots of Figure 4 in which the behavior open and closed Cell characteristics, averaged over all sites in all proteins in our dataset, are plotted against the *normalized* sequence evolutionary rates. For comparison, Figure 5 depicts the general behavior of the normalized site-specific evolutionary rates versus site-specific sequence entropy, $\Delta\Delta G$ rate, RSA, WCN, average Side-Chain B factor, Hydrogen bond strengths.

3.1 Average Side-Chain Coordinates as the Best Representation of Protein 3D Structure

Depending on the choice of the Cartesian coordinates used, there exist degeneracy in the definition of some site-specific structural variables. For example, the quantity WCN is generally calculated from the coordinates of C_α atoms in the 3-dimensional structure of protein. The choice of C_α coordinates is however mainly driven by convenience in WCN calculation and there is no reason to believe this set of atomic coordinates is the best representative of individual sites in proteins. Indeed, some earlier works have already suggested the use of center-of-mass of side chain coordinates to represent the 3D structure of protein Soyer et al. (2000). More recently, Marcos & Echave (2014) Marcos and Echave (2014) have also shown that WCN calculated from side-chain center-of-mass coordinates generally result in significantly better correlations of WCN with sequence variability measures.

Despite the highly popular choice of C_α atomic B factor as a proxy measure of residue flexibility Halle (2002), same definition degeneracy also exists on choice of atomic B factors that are used to represent site-specific flexibility. In addition to WCN and B factor, there is also ambiguity as to which set of residue atomic coordinates best represent individual sites in proteins for the generation of Voronoi polyhedra.

Here in this work, all possible choices of the representative set of atomic coordinates are considered in order to identify which set of atomic coordinates best represents individual sites for the calculation of WCN, B factor, and Voronoi cells. Depending on the set of atomic coordinates that represent the protein structure, there are at least 7 different measures of each individual site-specific structural properties, such as the Weighted Contact Number, B factor and Voronoi cell properties. These include the set of coordinates of all backbone atoms (N , C , C_α , O) and the first heavy atom in the amino acid side chains (C_β). In addition, representative coordinates for each site in protein are calculated by averaging over the coordinates of all heavy atoms in the side chains. Also calculated is a representative coordinate for each site by averaging over all heavy atom coordinates in the side chain and the backbone of the amino acid together. In rare cases where the side chain C_β atom had not been resolved in the PDB file or the amino acid lacked C_β (e.g., Glycine), the C_β coordinate for the specific amino acid were replaced with the coordinate of the corresponding C_α atom in the same amino acid. The resulting Spearman’s correlation strengths of site-specific evolutionary rates, sequence entropy, $\Delta\Delta G$ rate, Relative Solvent Accessibility (RSA), amino acid hydrophobicity, and Hydrogen bond energy with different measures of WCN, B factor, and Voronoi cell area are depicted in the plots of Figures 6, 8, and 7 respectively, for different sets of atomic coordinates used in the calculations. The hydrophobicity scales of amino acids residing in individual sites in proteins were taken from Hessa et al. (2005). Other hydrophobicity scales were also considered Wimley and White (1996); Kyte and Doolittle (1982), however similar results are obtained for all.

For the measure of local packing density in proteins (the Weighted Contact Number) we find that among all possible set of coordinates, the average over coordinates of all heavy atoms of each individual side chain results in WCN values that show the strongest correlation strength with other structural

and sequence properties, such as RSA, Voronoi cell properties, sequence entropy, and evolutionary rates. Specifically, WCN from average side chain coordinates outperforms WCN based on C_α coordinates in predicting RSA, $\Delta\Delta G$ rate, sequence entropy and evolutionary rates with median Spearman correlation differences of 0.09, 0.10, 0.07 & 0.08, respectively (Figure 6).

Similar to WCN, the Voronoi cell properties, most importantly the cell surface area, volume, edge length, eccentricity and the cell sphericity also correlate best with other structure and sequence properties, only if the geometric average of side chain coordinates are used as the seeds of Voronoi cells. Specifically, cell area from average side chain coordinates outperforms cell area based on C_α coordinates in predicting RSA, $\Delta\Delta G$ rate, sequence entropy and evolutionary rates with median Spearman correlation differences of 0.04, 0.06, 0.04 & 0.04, respectively (Figure 7).

It is notable that the standard deviations of the difference distributions for both quantities: WCN, and Voronoi cell area, are an order of magnitude smaller than the observed differences, implying that the correlation coefficients for all proteins in dataset uniformly translate to higher values by moving from C_α atomic coordinates to the geometric centers of the side chains, regardless of the strength of the correlation coefficients.

3.2 Average Side-Chain B Factors as the Best Representation of Local Fluctuations of Amino Acids in Proteins

For the measure of local flexibility in proteins (B factor) we similarly find that among all 7 representative measures of site B factors, the average of B factor values over all heavy atoms of each individual side chain results in the best correlations with other structural and sequence properties. Specifically, the average side chain B factor outperforms the commonly used C_α B factor in predicting RSA, $\Delta\Delta G$ rate, sequence entropy and evolutionary rates by a median Spearman correlation difference of 0.11, 0.12, 0.08 & 0.09, respectively (Figure 8).

The observed improvements in correlations of average side-chain B factor (vs. C_α B factor) with other structural properties also merit further attention. It was discussed in Section 3.1 and depicted in the plots of Figure 8 that in general, as one moves from the B factors of atoms in the backbone of amino acid to the B factor of side-chain atoms, the correlations of B factor with other site-specific structural and sequence properties improve. In particular, the use of average side-chain B factor turned out to result in the highest correlation strengths with other site-specific properties, implying that this average B factor is likely the best representation of the overall amino acid fluctuations and flexibility in a given site in protein. The definition of B factor and its derivation from Debye-Waller factor has been already discussed in Chapter ??, Eqns. ??–??.

The mean-square-displacement $\langle u^2 \rangle$ in Eqn. ?? can be decomposed into four contributing components Frauenfelder et al. (1979),

$$\langle u^2 \rangle = \langle u^2 \rangle_c + \langle u^2 \rangle_d + \langle u^2 \rangle_{ld} + \langle u^2 \rangle_v, \quad (4)$$

in which subscripts c, d, ld, v refer to fluctuations due to conformational substates, diffusion, lattice disorder, and thermal vibrations respectively. The second term $\langle u^2 \rangle_d$ is generally negligible and can be ignored in Eqn. 5. Of particular interest to this study is the first term, which is also typically the major contributor to the overall value of the atomic B factor, specially in high-resolution X-ray crystallography of proteins. This term represents the positional displacements of the atom of interest together with other atoms in the amino acid between many different conformational substates of the protein, with the transition probability between the substates governed by the Boltzmann distribution. Compared to atomic

coordinates, there are comparatively fewer restraints on the atomic B factors during X-ray crystallography refinement process, and thus in this regard B factor is generally considered as the *error sinks* for static and dynamic disorder and various kinds of model errors in the refinement process Read (1990). The noise and model uncertainty contributions to the atomic B factors in particular increase with decreasing the resolution of the X-ray crystallography. Better resolution in general corresponds to lower average B factors for the entire structure of the protein Read (1990).

Although the extraction of conformational fluctuations from noise in B factors seems a daunting task Read (1990), the effects of noise, model error and uncertainties due to limited X-ray crystallography resolution can be minimized by averaging B factors over the entire amino acid in a given site: To expand on this, consider the contribution of conformational fluctuations between different substates to be approximately the same for all atoms in the amino acid. The conformational fluctuations can be regarded as the collective motion of all atoms in the amino acid, on top of which there are noise fluctuations in each of the atoms. These collective motions are the type of fluctuations in B factors that are expected to reflect the biologically relevant and important factors for the proper functioning of the protein. The stochastic noise in the fluctuations is often assumed to have an isotropic Gaussian origin. Therefore, averaging over the atomic B factors in each individual amino acid essentially results in higher Signal-to-Noise Ratio (SNR) in the measurement of the amino acid conformational fluctuations. Figure 9 illustrates how this averaging over all atomic B factors increases the SNR in measuring the fluctuations due to conformational substate transitions of the amino acid.

To expand further on this, a simple argument may be given to explain the observed strongly-positive approximately-linear correlation between the two parameters in the plot of Figure 9. The contributions to the atomic B factor values of the i^{th} atom in the amino acid in the j^{th} site in a given protein can be assumed to originate from two major sources: conformational substates and stochastic noise due to model uncertainties in refinement process and limited resolution of the X-ray crystallography,

$$\langle u^2 \rangle_{ij} = \langle u^2 \rangle_{\text{substates},ij} + \langle u^2 \rangle_{\text{noise},ij}. \quad (5)$$

For simplicity and without loss of generality, one can assume that the contribution of fluctuations due to conformational substate transitions is approximately the same for all atomic B factors in a given amino acid residing the j^{th} site. In other words, the term $\langle u^2 \rangle_{\text{substates},ij}$ in the above equation has almost the same value $\langle u^2 \rangle_{\text{substates},j}$ for all atoms in the amino acid in the j^{th} site in protein. Thus, the average B factor for the entire amino acid molecule of size N_j atoms would be,

$$\begin{aligned} \langle u^2 \rangle_j &= \frac{1}{N_j} \sum_{i=1}^{N_j} \langle u^2 \rangle_{\text{substates},ij} + \langle u^2 \rangle_{\text{noise},ij} \\ &= \langle u^2 \rangle_{\text{substates},j} + \frac{1}{N_j} \sum_{i=1}^{N_j} \langle u^2 \rangle_{\text{noise},ij} \\ &= \langle u^2 \rangle_{\text{substates},j} + \frac{1}{N_j} \sum_{i=1}^{N_j} \mu_{\text{noise},j} \end{aligned} \quad (6)$$

in which $\mu_{\text{noise},j}$ is the average noise in the j^{th} amino acid. The ratio of the B factor of the ij^{th} atom to the average B factor of the j^{th} site in protein can be approximated as,

$$\frac{\langle u^2 \rangle_{ij}}{\langle u^2 \rangle_j} \simeq \frac{\langle u^2 \rangle_{substates,j} + \langle u^2 \rangle_{noise,ij}}{\langle u^2 \rangle_{substates,j} + \mu_{noise,j}} \quad (7)$$

$$= \frac{1}{1 + \mu_{noise,j}/\langle u^2 \rangle_{substates,j}} + \left(\frac{\langle u^2 \rangle_{noise,ij}}{\langle u^2 \rangle_{substates,j}} \right) \frac{1}{1 + \mu_{noise,j}/\langle u^2 \rangle_{substates,j}} \quad (8)$$

$$\simeq 1 - \frac{\mu_{noise,j}}{\langle u^2 \rangle_{substates,j}}, \quad (9)$$

where from line 8 to 9, an assumption was made that the second term in line 8 could be neglected compared to the first term and that the noise compared to conformational fluctuation is small, that is, $\mu_{noise,j}/\langle u^2 \rangle_{substates,j} < 1$ (an error of 0.2\AA corresponds approximately to 1\AA increase in B factor Read (1990)). Knowing that the average noise across different amino acids is approximately the same Frauenfelder et al. (1979), that is $\mu_{noise,j} \sim \mu_{noise}$, and that the noise due to X-ray crystallography almost negatively linearly correlates with crystallography resolution in the range $\sim 1 - 3 [\text{\AA}]$ Read (1990), that is $\mu_{noise} \propto -\text{resolution}$, a positive approximately-linear relationship between the average of the B factor ratios over the entire amino acids in the protein structure and the X-ray crystallography resolution would be obtained,

$$\frac{BF_C}{BF_{AA}} = \frac{1}{L} \sum_{j=1}^L \frac{\langle u^2 \rangle_{ij}}{\langle u^2 \rangle_j} \quad (10)$$

$$\propto -\mu_{noise} \sum_{j=1}^L \frac{1}{\langle u^2 \rangle_{substates,j}} \quad (11)$$

$$\propto \text{resolution} \quad (12)$$

in which L represents the length of the protein sequence. The summation term in line 11 would not influence this linear relationship, causing only scatter in the relation, so long as the length of the protein not does impose limitations on the resolution of X-ray crystallography of proteins. In general, however this may not be the case. For the sample of 209 proteins considered here, there exists indeed a weak Spearman's correlation coefficient of $\rho \sim 0.2$ between protein length (L) and resolution. Figure 9 illustrates the relationship between the average B factors ratio and the resolution in the dataset, using atom C in the backbone of all amino acids in proteins representing the i^{th} atom in the notation of Eqn. 10. It is also notable that the the atomic fluctuations due to conformational substates may not be exactly the same for all atoms in an amino acid in a given site in protein. Indeed, one may expect the conformational fluctuations in the backbone atoms would be less significant compared to conformational fluctuations of side-chain atoms.

Although averaging B factor over the entire amino acid atoms would reduce the noise further than averaging over side-chain atoms, the functionally important conformational fluctuations that are better captured by the side-chain atomic B factors would compensate for the increase in the noise, such that overall, the B factors averaged over side-chain atoms results in slightly better correlations with sequence variability and other relevant structural characteristics depicted in Figure 8.

Effects of Long-Range Amino Acid Interactions on Sequence Variability

Throughout the previous sections, a variety of site-specific structural characteristics of proteins were calculated and discussed, using different sets of atomic coordinates representing individual sites in proteins. These include the weighted contact number, the Voronoi cell characteristics, and representative

site-specific B factor. To make comprehensive comparison of all site-specific structural properties of proteins, we also calculate the Relative Solvent Accessibility (RSA) and $\Delta\Delta G$ rate (e.g., Echave et al., 2014) of individual amino acids in their sites in proteins.

Figure 10 & 11 compare the predictive power of each of site-specific structural quantities about sequence variability as measured by evolutionary rates (r_4sJC) and sequence entropy. It is notable that once WCN is recalculated using the geometric center of the side chains as the representative coordinates of individual sites, the quantity WCN still outperforms all other structural quantities, including those derived from Voronoi tessellation, in explaining site-specific sequence variability. The better performance of WCN compared to local packing density as measured from Voronoi cell volume and area may not be surprising, since WCN by its definition takes into account the potential long-range interactions among amino acids in different regions of protein. Indeed, the fractal dimension of proteins very much resembles that of lattice percolation models Stauffer and Aharony (1994) and similarly the random packing of hard spheres near percolation threshold Lorenz et al. (1993); Liang and Dill (2001). To expand on this, define the average maximum extent of a protein as,

$$R_m = \frac{1}{2d} \sum_{i=1}^d (x_{i,max} - x_{i,min}), \quad (13)$$

in which $d = 3$ is the dimension of the Euclidean space $x_{i,max} - x_{i,min}$ is the maximum physical extent of the protein, as represented by the geometric center of the side-chain coordinates, in each of the three spatial dimensions. Alternatively, the radius of gyration of a protein of length N can be defined as (similar to that of a finite size cluster: Egn. 45a, Sec. 3.2, in Stauffer and Aharony (1994)),

$$R_g = \sqrt{\sum_{i=1}^N \frac{|\vec{r}_i - \vec{r}_0|^2}{N}}, \quad (14)$$

where,

$$\vec{r}_0 = \sum_{i=1}^N \frac{\vec{r}_i}{N}, \quad (15)$$

is the geometric center of the protein, and r_i is the position of the geometric center of the side-chain of the i^{th} amino acid in protein. This definition is such that the kinetic energy and the angular momentum of the protein about the \vec{r}_0 is equivalent to the kinetic energy and the angular momentum of all amino acids residing on a ring of radius R_g centered at \vec{r}_0 . Figure 12 & 13 depict the behavior of the maximum extent (R_m) versus protein volume (V) and the radius of gyration (R_g) versus the protein length (N), respectively.

The protein volumes and surface areas calculated using βV software Voss and Gerstein (2010). A symmetric linear fit (i.e., Deming regression) to the plot of $\log R_m$ vs. $\log V$ and $\log R_g$ vs. $\log N$ results in regression slopes of $D \simeq 2.47 \pm 0.06$ & $D \simeq 2.60 \pm 0.08$ respectively. The observed exponents are very similar to those of the scaling relation,

$$V \propto R^D, \quad (p \simeq p_c) \quad (16)$$

with $D \simeq 2.51 \pm 0.01$ in numerical simulations of hard-sphere packing Lorenz et al. (1993) in three dimensions near percolation threshold ($p \simeq p_c$) or the exponents derived from lattice models $D \simeq 2.54 \pm 0.05$ Adler et al. (1990) & $D \simeq 2.5$ Stauffer and Aharony (1994). It is notable that far from percolation threshold (i.e., $p \rightarrow 0$) in three dimensions, $D = 2$ Parisi and Sourlas (1981), while above the threshold ($p > p_c$), $D = d = 3$, in 3D space.

ACKNOWLEDGEMENTS

We thank Austin G. Meyer, Stephanie Spielman and Eleisha Jackson at UT Austin for helpful discussions and comments.

References

- Adler J, Meir Y, Aharony A, Harris AB. 1990. Series study of percolation moments in general dimension. *Physical Review B*. 41:9183–9206.
- Ashkenazy H, Erez E, Martz E, Pupko T, Ben-Tal N. 2010. ConSurf 2010: calculating evolutionary conservation in sequence and structure of proteins and nucleic acids. *Nucleic Acids Research*. 38:W529–W533.
- Bloom JD, Drummond DA, Arnold FH, Wilke CO. 2006. Structural Determinants of the Rate of Protein Evolution in Yeast. *Molecular Biology and Evolution*. 23:1751–1761.
- Bustamante CD, Townsend JP, Hartl DL. 2000. Solvent Accessibility and Purifying Selection Within Proteins of Escherichia coli and Salmonella enterica. *Molecular Biology and Evolution*. 17:301–308.
- Conant GC, Stadler PF. 2009. Solvent Exposure Imparts Similar Selective Pressures across a Range of Yeast Proteins. *Molecular Biology and Evolution*. 26:1155–1161.
- Echave J, Jackson EL, Wilke CO. 2014. Relationship between protein thermodynamic constraints and variation of evolutionary rates among sites. *bioRxiv*. p. 009423.
- Franzosa EA, Xia Y. 2009. Structural Determinants of Protein Evolution Are Context-Sensitive at the Residue Level. *Molecular Biology and Evolution*. 26:2387–2395.
- Frauenfelder H, Petsko GA, Tsernoglou D. 1979. Temperature-dependent X-ray diffraction as a probe of protein structural dynamics. *Nature*. 280:558–563.
- Gerstein M, Sonnhammer ELL, Chothia C. 1994. Volume changes in protein evolution. *Journal of Molecular Biology*. 236:1067–1078.
- Goldenberg O, Erez E, Nimrod G, Ben-Tal N. 2009. The ConSurf-DB: pre-calculated evolutionary conservation profiles of protein structures. *Nucleic Acids Research*. 37:D323–D327.
- Goldman N, Thorne JL, Jones DT. 1998. Assessing the Impact of Secondary Structure and Solvent Accessibility on Protein Evolution. *Genetics*. 149:445–458.
- Halle B. 2002. Flexibility and packing in proteins. *Proceedings of the National Academy of Sciences*. 99:1274–1279.
- Hamelryck T. 2005. An amino acid has two sides: A new 2d measure provides a different view of solvent exposure. *Proteins: Structure, Function, and Bioinformatics*. 59:38–48.
- Hessa T, Kim H, Bihlmaier K, Lundin C, Boekel J, Andersson H, Nilsson I, White SH, von Heijne G. 2005. Recognition of transmembrane helices by the endoplasmic reticulum translocon. *Nature*. 433:377–381.
- Huang TT, Marcos MLdV, Hwang JK, Echave J. 2014. A mechanistic stress model of protein evolution accounts for site-specific evolutionary rates and their relationship with packing density and flexibility. *BMC Evolutionary Biology*. 14:78.
- Kabsch W, Sander C. 1983. Dictionary of protein secondary structure: Pattern recognition of hydrogen-bonded and geometrical features. *Biopolymers*. 22:2577–2637.

- Katoh K, Kuma Ki, Toh H, Miyata T. 2005. MAFFT version 5: improvement in accuracy of multiple sequence alignment. *Nucleic Acids Research*. 33:511–518.
- Kyte J, Doolittle RF. 1982. A simple method for displaying the hydropathic character of a protein. *Journal of Molecular Biology*. 157:105–132.
- Liang J, Dill KA. 2001. Are Proteins Well-Packed? *Biophysical Journal*. 81:751–766.
- Liao H, Yeh W, Chiang D, Jernigan R, Lustig B. 2005. Protein sequence entropy is closely related to packing density and hydrophobicity. *Protein engineering, design & selection : PEDS*. 18:59–64.
- Lin CP, Huang SW, Lai YL, Yen SC, Shih CH, Lu CH, Huang CC, Hwang JK. 2008. Deriving protein dynamical properties from weighted protein contact number. *Proteins: Structure, Function, and Bioinformatics*. 72:929–935.
- Liu Y, Bahar I. 2012. Sequence Evolution Correlates with Structural Dynamics. *Molecular Biology and Evolution*. 29:2253–2263.
- Lorenz B, Orgzall I, Heuer HO. 1993. Universality and cluster structures in continuum models of percolation with two different radius distributions. *Journal of Physics A: Mathematical and General*. 26:4711.
- Marcos ML, Echave J. 2014. Too packed to change: site-specific substitution rates and side-chain packing in protein evolution. *bioRxiv*. p. 013359.
- Mayrose I, Graur D, Ben-Tal N, Pupko T. 2004. Comparison of Site-Specific Rate-Inference Methods for Protein Sequences: Empirical Bayesian Methods Are Superior. *Molecular Biology and Evolution*. 21:1781–1791.
- Meyer AG, Dawson ET, Wilke CO. 2013. Cross-species comparison of site-specific evolutionary-rate variation in influenza haemagglutinin. *Philosophical Transactions of the Royal Society of London B: Biological Sciences*. 368:20120334.
- Meyer AG, Wilke CO. 2013. Integrating Sequence Variation and Protein Structure to Identify Sites under Selection. *Molecular Biology and Evolution*. 30:36–44.
- Meyer AG, Wilke CO. 2015. Geometric constraints dominate the antigenic evolution of influenza H3n2 hemagglutinin. *bioRxiv*. p. 014183.
- Murzin AG, Brenner SE, Hubbard T, Chothia C. 1995. SCOP: A structural classification of proteins database for the investigation of sequences and structures. *Journal of Molecular Biology*. 247:536–540.
- Parisi G, Sourlas N. 1981. Critical Behavior of Branched Polymers and the Lee-Yang Edge Singularity. *Physical Review Letters*. 46:871–874.
- Porter CT, Bartlett GJ, Thornton JM. 2004. The Catalytic Site Atlas: a resource of catalytic sites and residues identified in enzymes using structural data. *Nucleic Acids Research*. 32:D129–D133.
- Ramsey DC, Scherrer MP, Zhou T, Wilke CO. 2011. The Relationship Between Relative Solvent Accessibility and Evolutionary Rate in Protein Evolution. *Genetics*. 188:479–488.
- Read RJ. 1990. Structure-factor probabilities for related structures. *Acta Crystallographica Section A Foundations of Crystallography*. 46:900–912.
- Richards FM. 1974. The interpretation of protein structures: Total volume, group volume distributions and packing density. *Journal of Molecular Biology*. 82:1–14.

- Rodionov MA, Blundell TL. 1998. Sequence and structure conservation in a protein core. *Proteins: Structure, Function, and Bioinformatics*. 33:358–366.
- Rycroft CH. 2009. VORO++: A three-dimensional Voronoi cell library in C++. *Chaos: An Interdisciplinary Journal of Nonlinear Science*. 19:041111.
- Scherrer MP, Meyer AG, Wilke CO. 2012. Modeling coding-sequence evolution within the context of residue solvent accessibility. *BMC Evolutionary Biology*. 12:179.
- Shahmoradi A, Sydykova DK, Spielman SJ, Jackson EL, Dawson ET, Meyer AG, Wilke CO. 2014. Predicting Evolutionary Site Variability from Structure in Viral Proteins: Buriedness, Packing, Flexibility, and Design. *Journal of Molecular Evolution*. 79:130–142.
- Shenkin PS, Erman B, Mastrandrea LD. 1991. Information-theoretical entropy as a measure of sequence variability. *Proteins: Structure, Function, and Bioinformatics*. 11:297–313.
- Shih CH, Chang CM, Lin YS, Lo WC, Hwang JK. 2012. Evolutionary information hidden in a single protein structure. *Proteins: Structure, Function, and Bioinformatics*. 80:1647–1657.
- Sikosek T, Chan HS. 2014. Biophysics of protein evolution and evolutionary protein biophysics. *Journal of The Royal Society Interface*. 11:20140419.
- Soyer A, Chomilier J, Mornon JP, Jullien R, Sadoc JF. 2000. Voronoi Tessellation Reveals the Condensed Matter Character of Folded Proteins. *Physical Review Letters*. 85:3532–3535.
- Stauffer D, Aharony A. 1994. Introduction To Percolation Theory. CRC Press.
- Tien MZ, Meyer AG, Sydykova DK, Spielman SJ, Wilke CO. 2013. Maximum Allowed Solvent Accessibilities of Residues in Proteins. *PLoS ONE*. 8:e80635.
- Voss NR, Gerstein M. 2010. 3v: cavity, channel and cleft volume calculator and extractor. *Nucleic Acids Research*. 38:W555–W562.
- Webb EC. 1992. *Enzyme nomenclature 1992. Recommendations of the Nomenclature Committee of the International Union of Biochemistry and Molecular Biology on the Nomenclature and Classification of Enzymes*. pp. xiii + 863 pp.
- Wilke CO, Bloom JD, Drummond DA, Raval A. 2005. Predicting the Tolerance of Proteins to Random Amino Acid Substitution. *Biophysical Journal*. 89:3714–3720.
- Wimley WC, White SH. 1996. Experimentally determined hydrophobicity scale for proteins at membrane interfaces. *Nature Structural Biology*. 3:842–848.
- Xia F, Tong D, Yang L, Wang D, Hoi SCH, Koehl P, Lu L. 2014. Identifying essential pairwise interactions in elastic network model using the alpha shape theory. *Journal of Computational Chemistry*. 35:1111–1121.
- Yang L, Song G, Jernigan RL. 2009. Protein elastic network models and the ranges of cooperativity. *Proceedings of the National Academy of Sciences*. 106:12347–12352.
- Yeh SW, Huang TT, Liu JW, Yu SH, Shih CH, Hwang JK, Echave J. 2014a. Local Packing Density Is the Main Structural Determinant of the Rate of Protein Sequence Evolution at Site Level. *BioMed Research International*. 2014:e572409.
- Yeh SW, Liu JW, Yu SH, Shih CH, Hwang JK, Echave J. 2014b. Site-Specific Structural Constraints on Protein Sequence Evolutionary Divergence: Local Packing Density versus Solvent Exposure. *Molecular Biology and Evolution*. 31:135–139.

- Zhou W, Yan H. 2014. Alpha shape and Delaunay triangulation in studies of protein-related interactions. *Briefings in Bioinformatics*. 15:54–64.
- Zomorodian A, Guibas L, Koehl P. 2006. Geometric filtering of pairwise atomic interactions applied to the design of efficient statistical potentials. *Computer Aided Geometric Design*. 23:531–544.

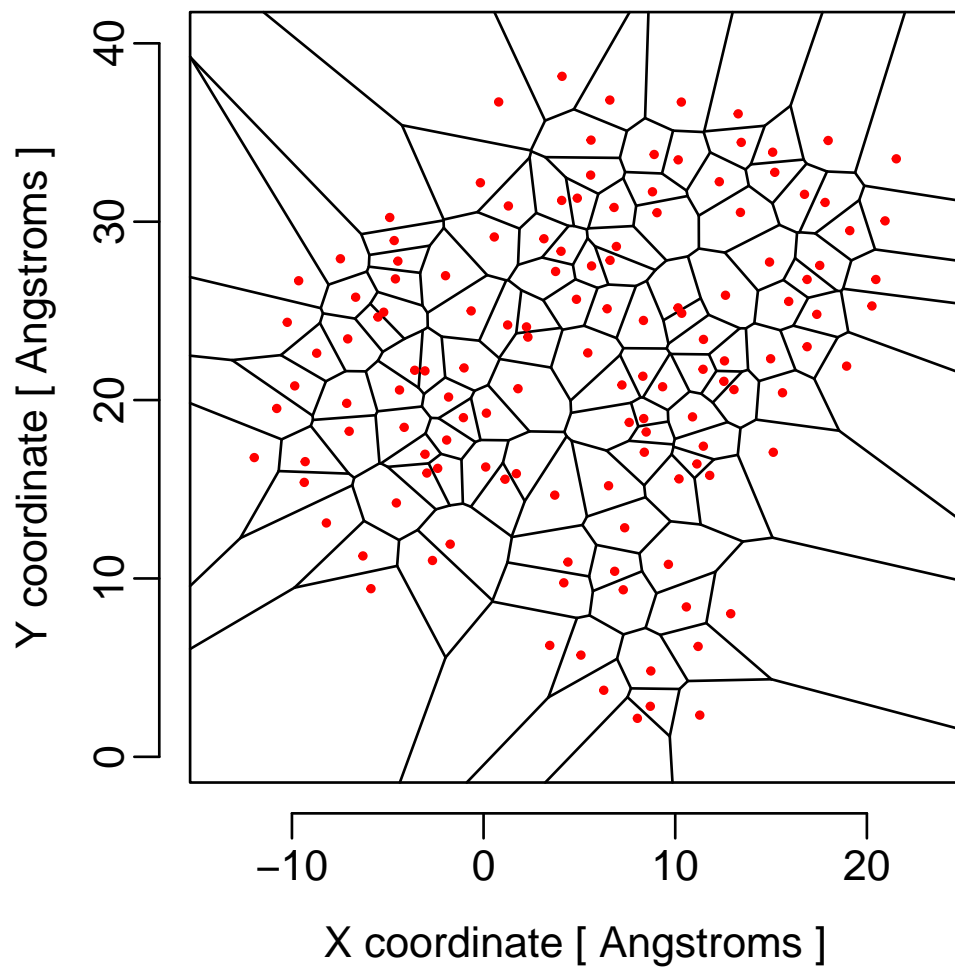


Figure 1: An Example 2-dimensional Voronoi diagram for bacteriophage T7 lysozyme (Protein Data Bank ID ‘1LBA’). The red dots represent the backbone C_α atoms projected on the X–Y plane, used as cell seeds in Voronoi tessellation.

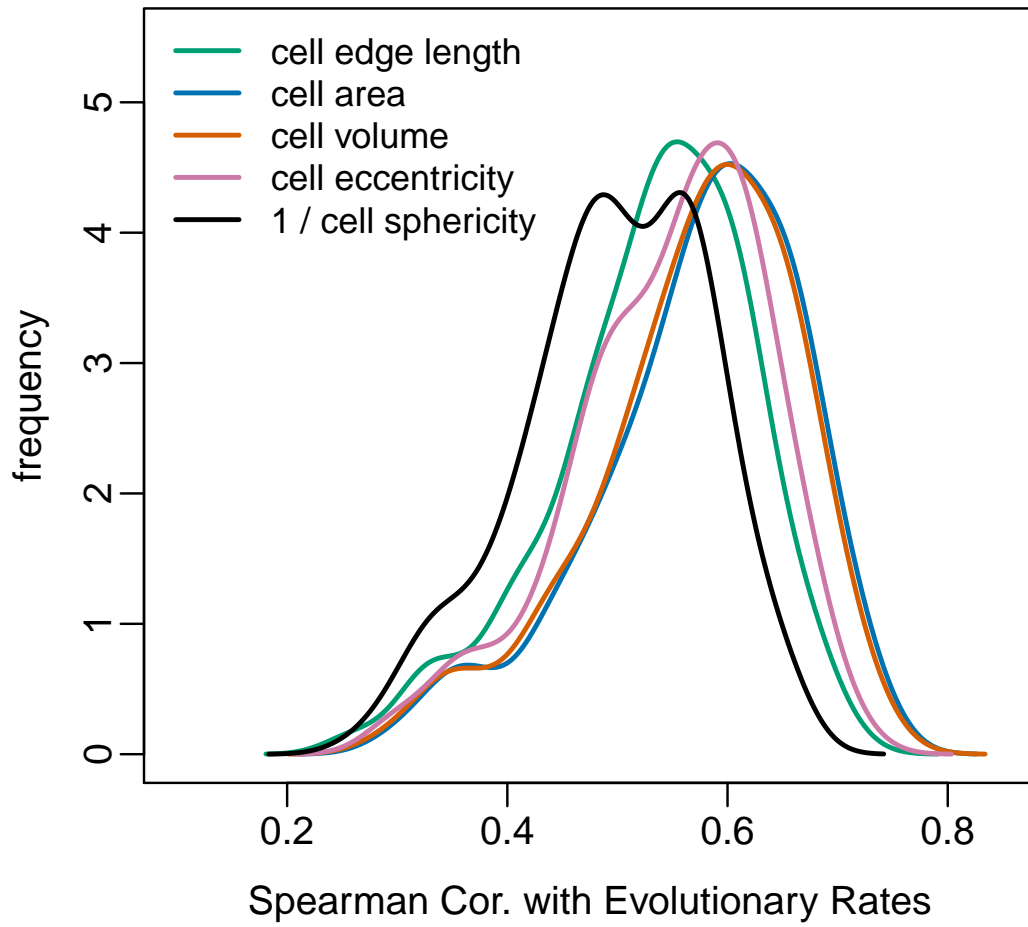


Figure 2: A comparison of the prediction power of different Voronoi cell characteristics about site-specific evolutionary rates (ER). Note that all cell characteristic correlate positively with ER, except sphericity which strongly negatively correlates with ER.

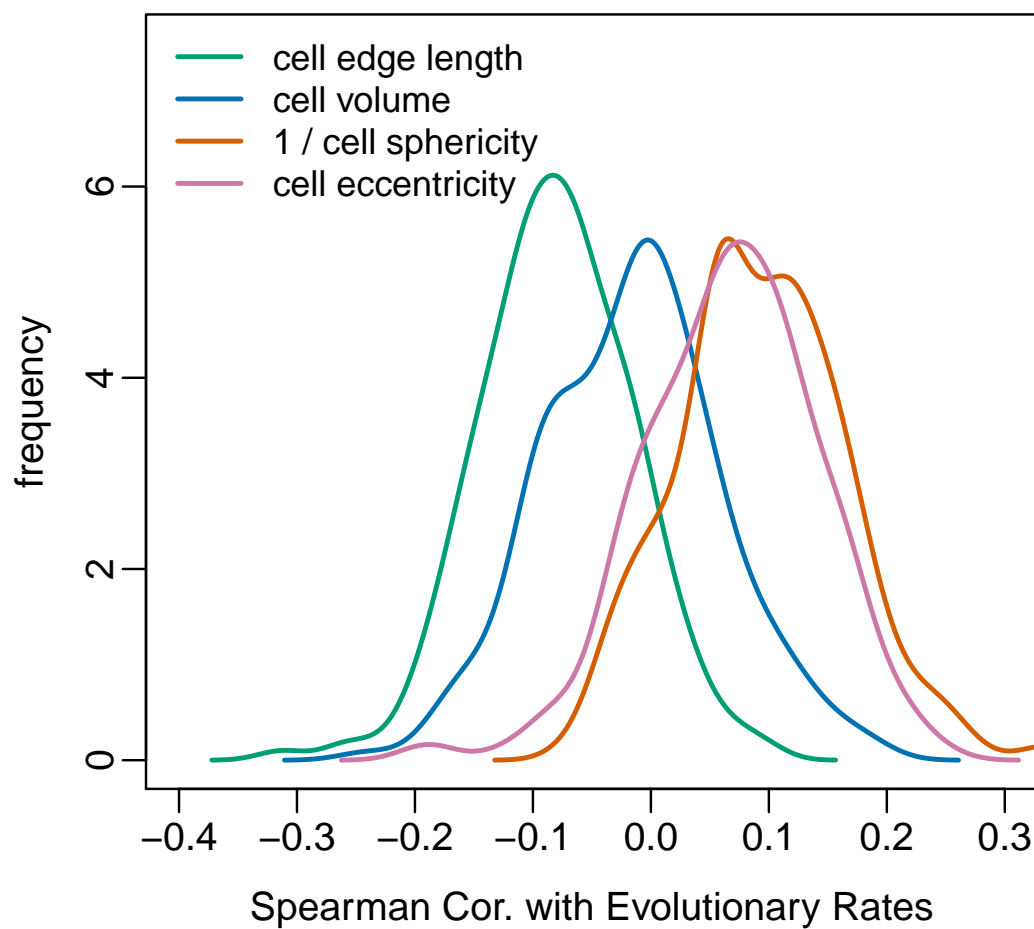


Figure 3: The partial correlation strengths of the same Voronoi cell characteristics with sequence evolutionary rates while controlling for the cell area.

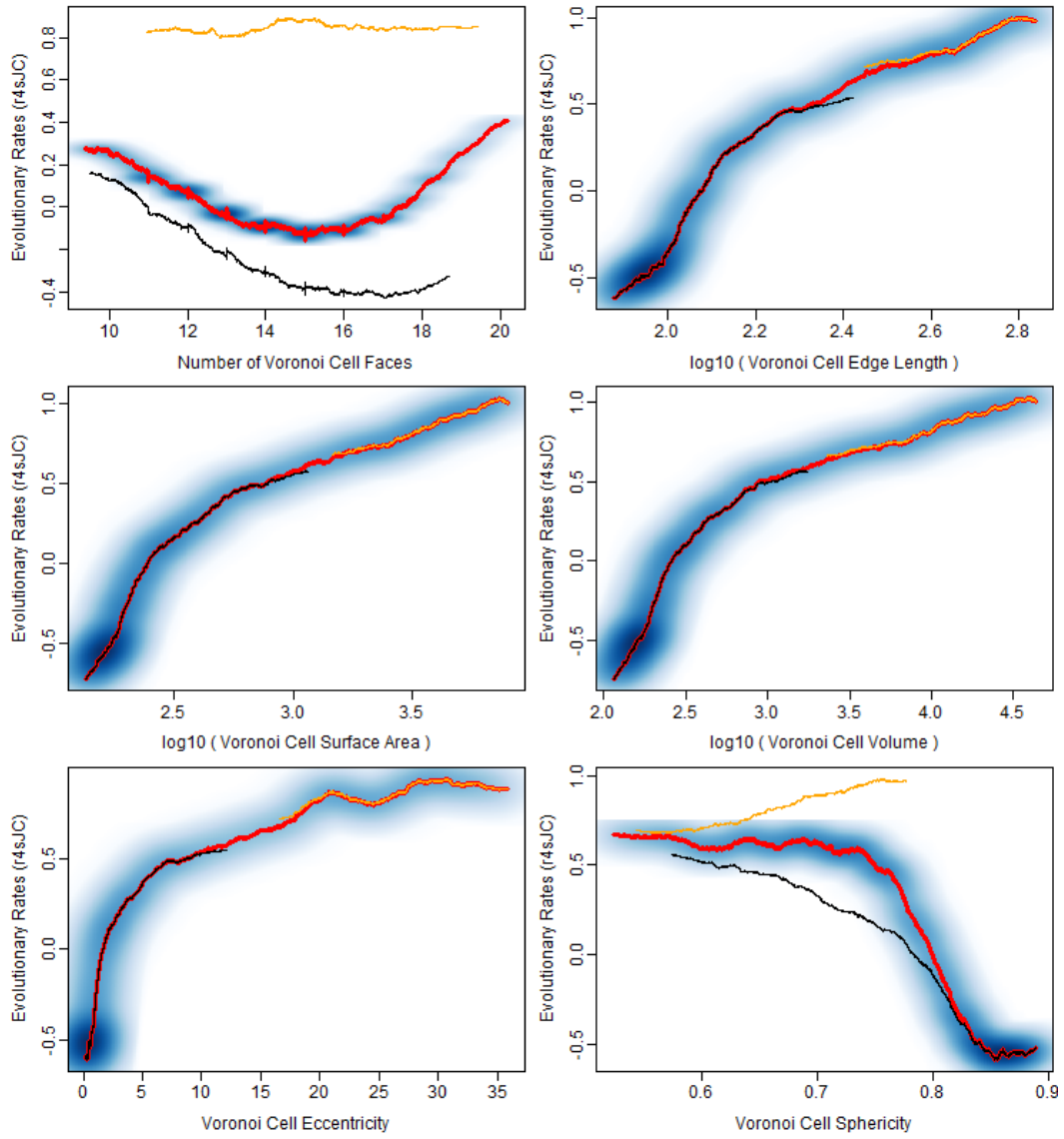


Figure 4: General behavior of Voronoi cell characteristics versus normalized site-specific evolutionary rates among all sites in all 209 proteins in dataset. The red curves in each plot is obtained by adjacent-averaging of every 3000 sites. The black & orange curves represent respectively the general behaviors of closed & open Voronoi cell characteristics. The background heat map in each plot is a 2D density plot of all 75755 amino acid sites in all 209 proteins, showing the overall distribution of sites about the average curve.

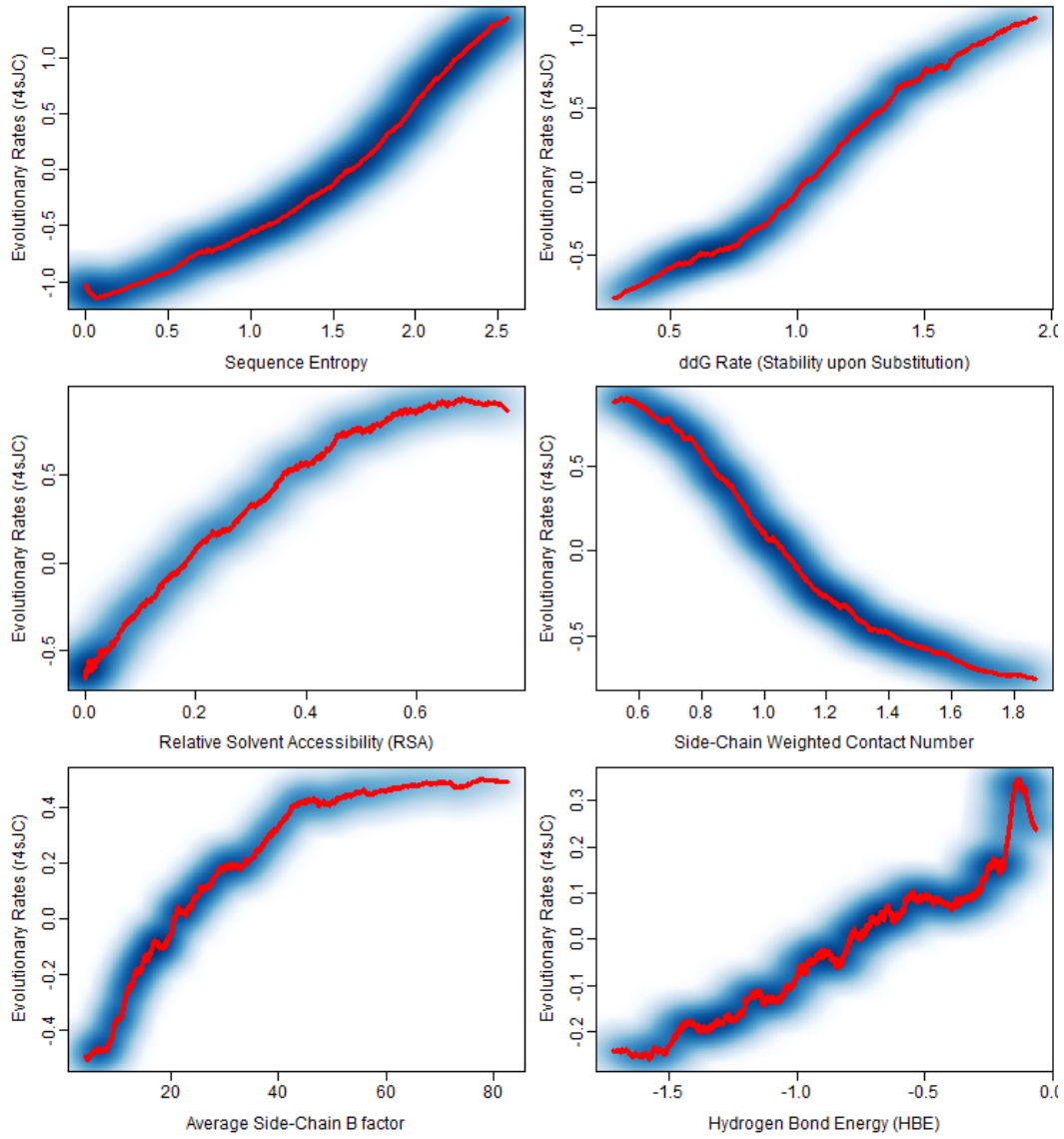


Figure 5: General behavior of site-specific structural characteristics versus site-specific evolutionary rates among all sites in all 209 proteins in dataset. The red curves in each plot is obtained by adjacent-averaging of every 3000 sites. The background heat map in each plot is a 2D density plot of all 75755 amino acid sites in all 209 proteins, showing the overall distribution of sites about the average curve.

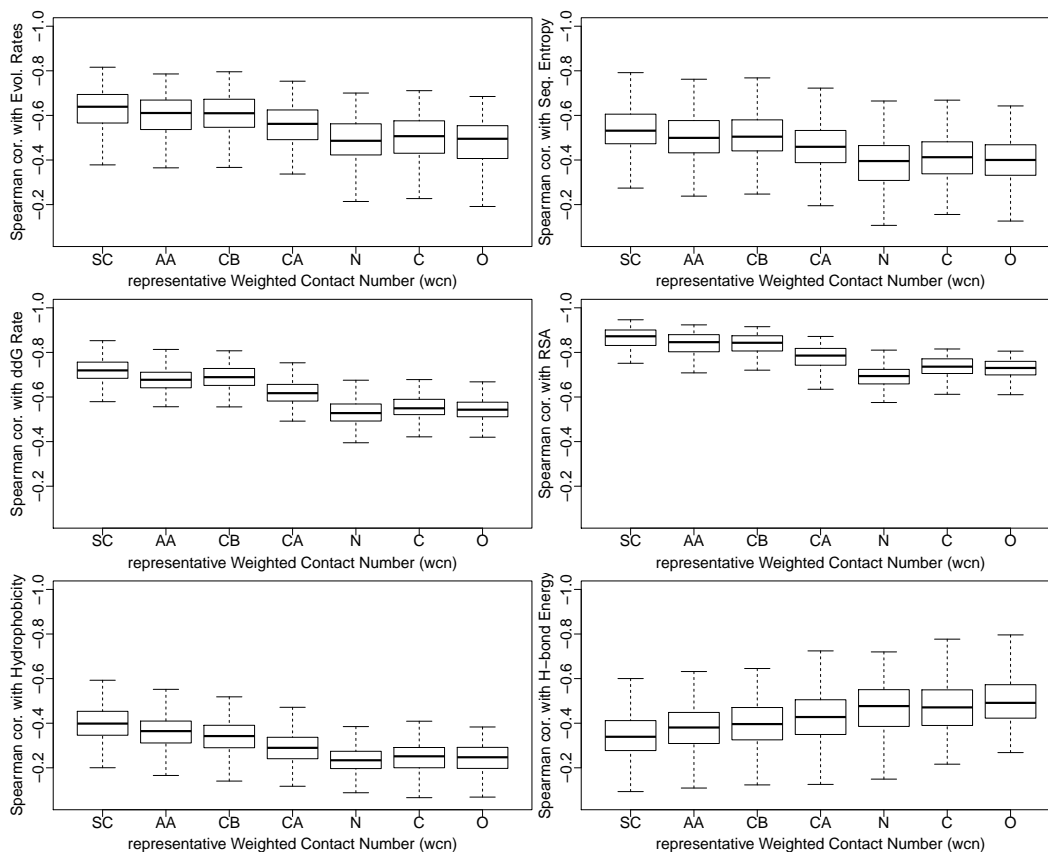


Figure 6: A comparison of the correlation strength of 6 different measures of Weighted Contact Number (WCN) with 6 coordinate-independent structural or sequence properties for 209 proteins in dataset. The contact numbers, WCN, are calculated using 6 sets of atomic coordinates: *SC*, *AA*, *CB*, *CA*, *N*, *C*, *O*, used as different representations of individual sites in proteins. The two labels *SC* & *AA* stand respectively for the geometric average coordinates of the Side Chain (SC) atoms and the entire Amino Acid (AA) atoms, excluding hydrogens.

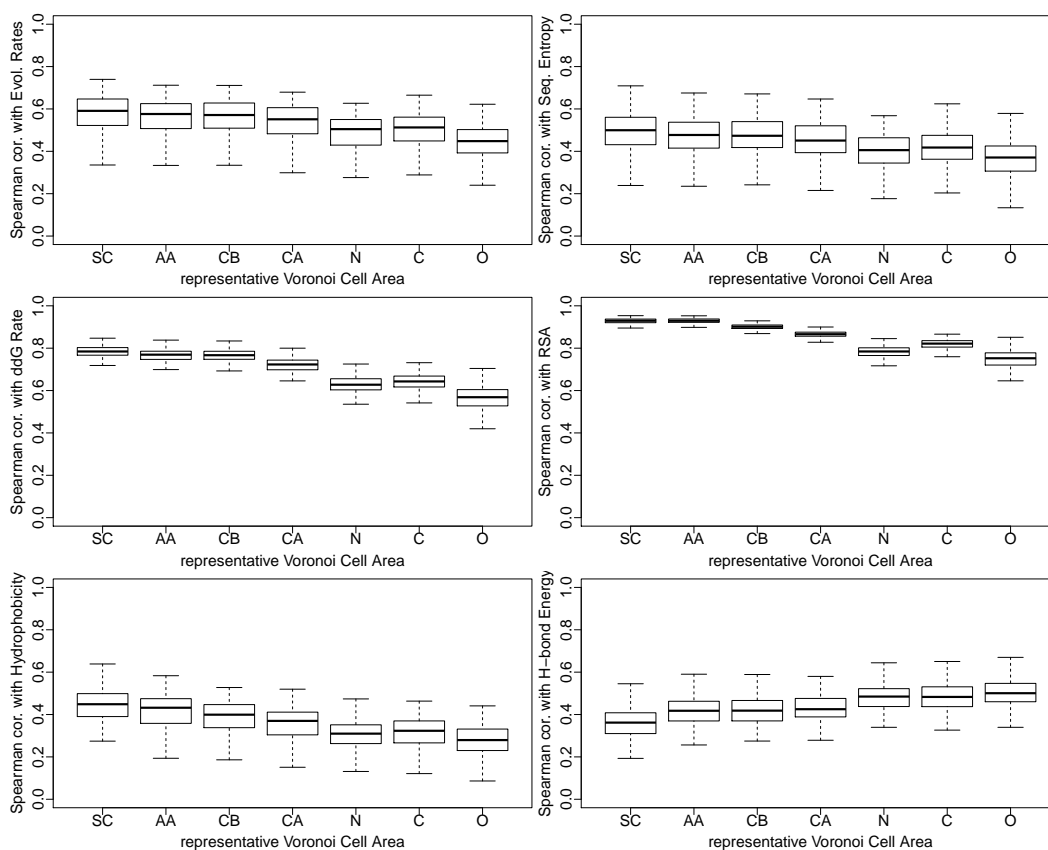


Figure 7: A comparison of the correlation strength of 6 different measures of Voronoi cell areas with 6 coordinate-independent structural or sequence properties for 209 proteins in dataset. The Voronoi cells are generated using 6 sets of atomic coordinates: *SC*, *AA*, *CB*, *CA*, *N*, *C*, *O*, used as different representations of individual sites in proteins. The two labels *SC* & *AA* stand respectively for the geometric average coordinates of the Side Chain (SC) atoms and the entire Amino Acid (AA) atoms, excluding hydrogens.

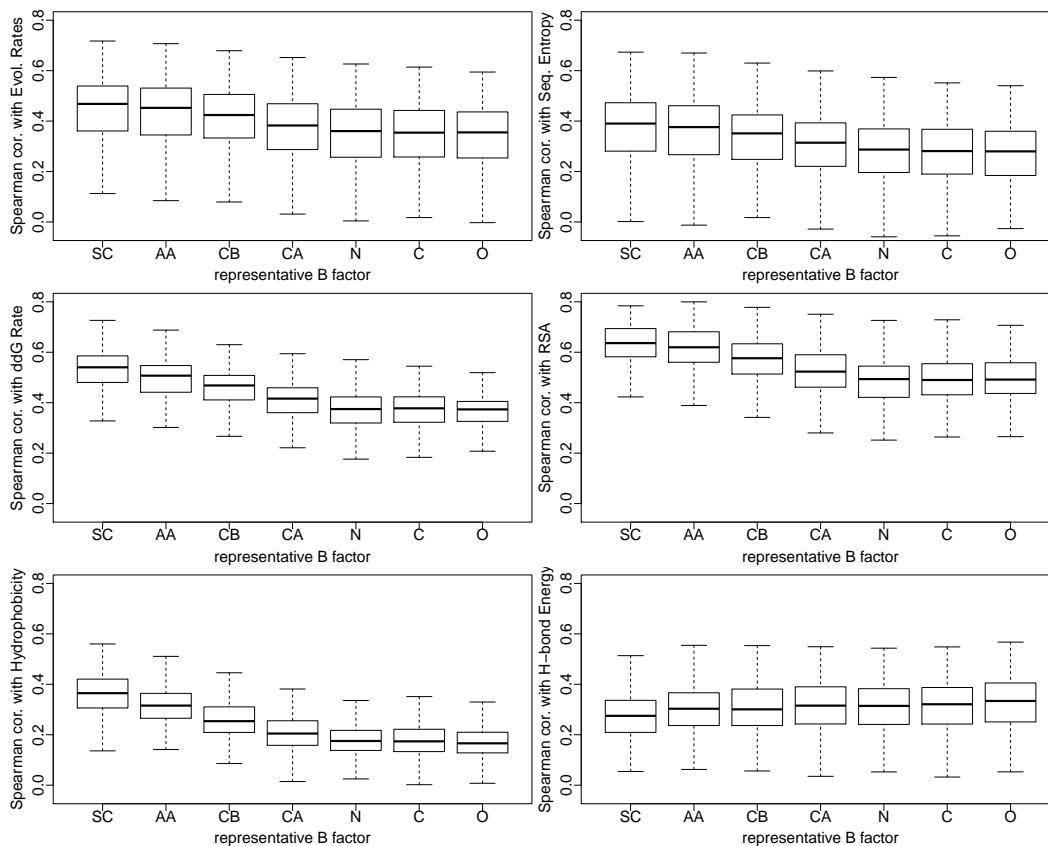


Figure 8: A comparison of the correlation strength of 6 different measures of B factor with 6 coordinate-independent structural or sequence properties for 209 proteins in dataset. Shown on the horizontal axes, are the 6 representative atomic B factors: *SC*, *AA*, *CB*, *CA*, *N*, *C*, *O* used as flexibility measures of individual sites in proteins. The two variables *SC* & *AA* stand respectively for the average B factor of all Side Chain (SC) atoms and the entire Amino Acid (AA) atoms, excluding hydrogens.

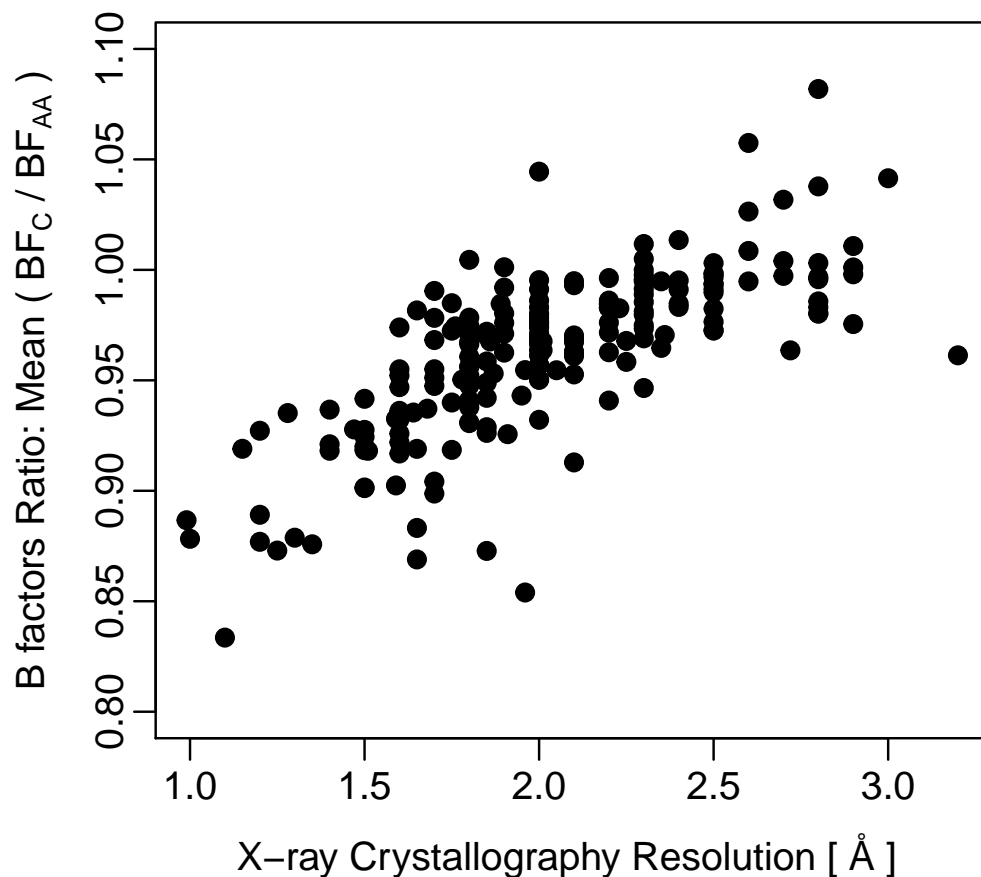


Figure 9: An illustration of the strong positive correlation of X-ray crystallography resolution with the ratio of the backbone C atomic B factor to the average amino acid B factor (BF_C/BF_{AA}), averaged over all sites in individual proteins, highlighting the significant contributions of noise and model errors to atomic B factor values. The Spearman's correlation coefficient between the two quantities is $\rho \sim 0.76$. No significant correlation would be expected in the absence of noise due to limited resolution of the X-ray crystallography of proteins. Each filled circle in the plot represents one protein in the dataset of 209 enzymes used in this work.

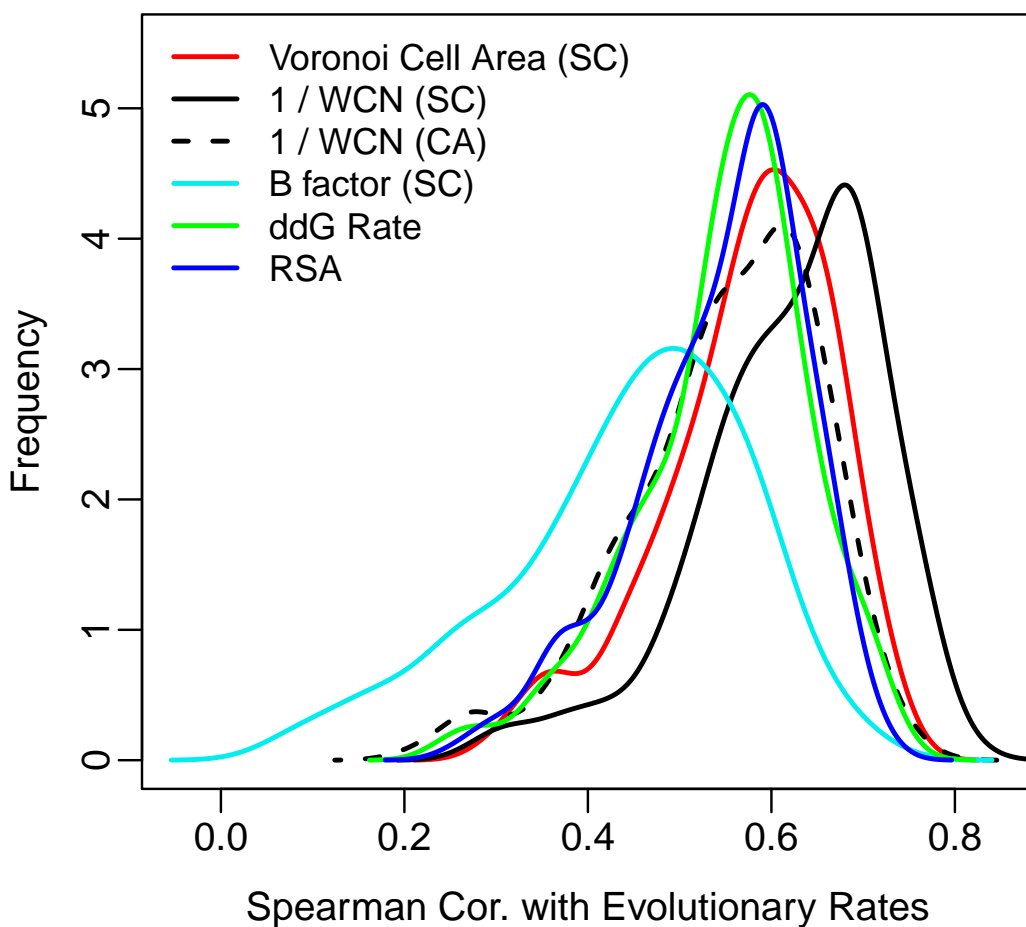


Figure 10: A comparison of the prediction power of five structural variables about site-specific evolutionary rates (ER). All structural quantities correlate positively with ER, with the exception of Weighted Contact Number (WCN) which correlates negatively. For better illustration however, the Spearman's correlation coefficient (ρ) of the inverse of WCN with ER are shown in the Figure. Note that the Spearman's ρ is a rank correlation coefficient, meaning that the use of inverse WCN only changes the sign and not the magnitude of ρ . The abbreviation *SC* refers to the use of average Side-Chain coordinates or average Side-Chain B factor wherever used, and *CA* refers to the use of backbone C_α atomic coordinates for representation of individual sites in proteins.

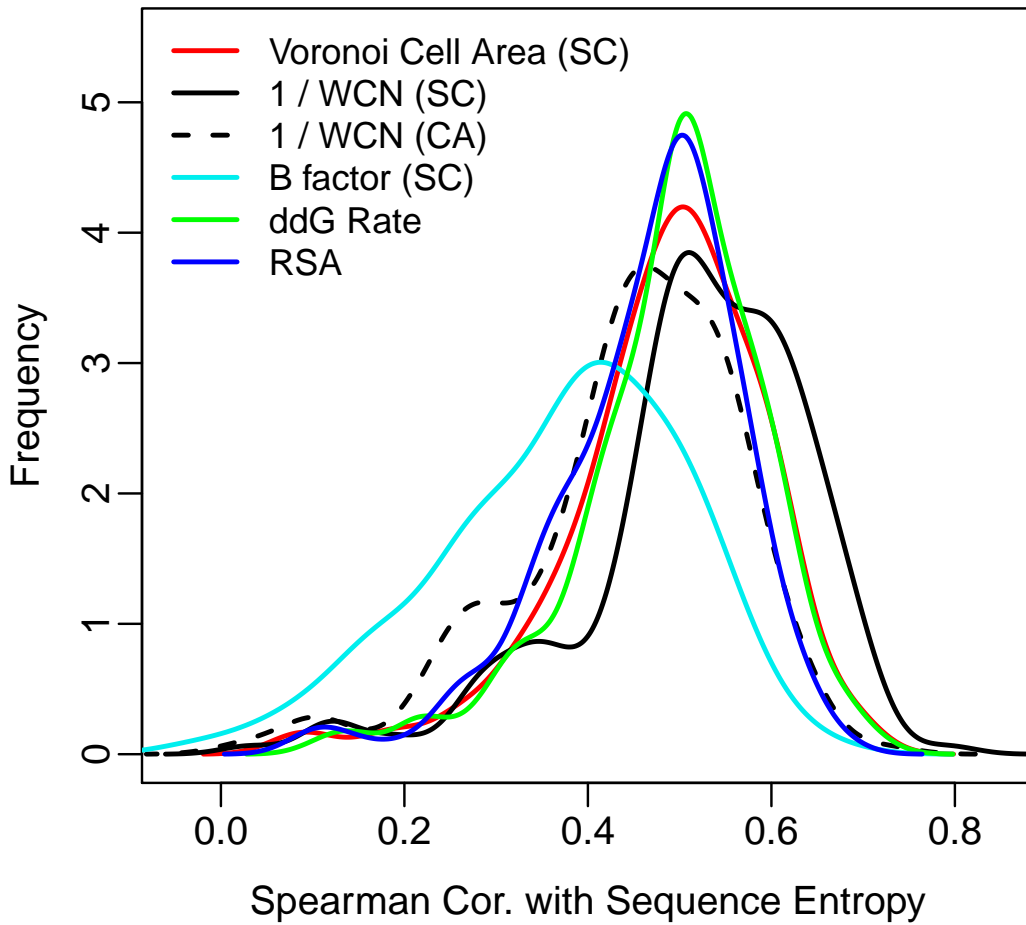


Figure 11: A comparison of the prediction power of five structural variables about site-specific Sequence Entropy (SE). All structural quantities correlate positively with SE, with the exception of Weighted Contact Number (WCN) which correlates negatively. For better illustration however, the Spearman's correlation coefficient (ρ) of the inverse of WCN with ER are shown in the Figure. Note that the Spearman's ρ is a rank correlation coefficient, meaning that the use of inverse WCN only changes the sign and not the magnitude of ρ . The abbreviation *SC* refers to the use of average Side-Chain coordinates or average Side-Chain B factor wherever used, and *CA* refers to the use of backbone C_α atomic coordinates for representation of individual sites in proteins.

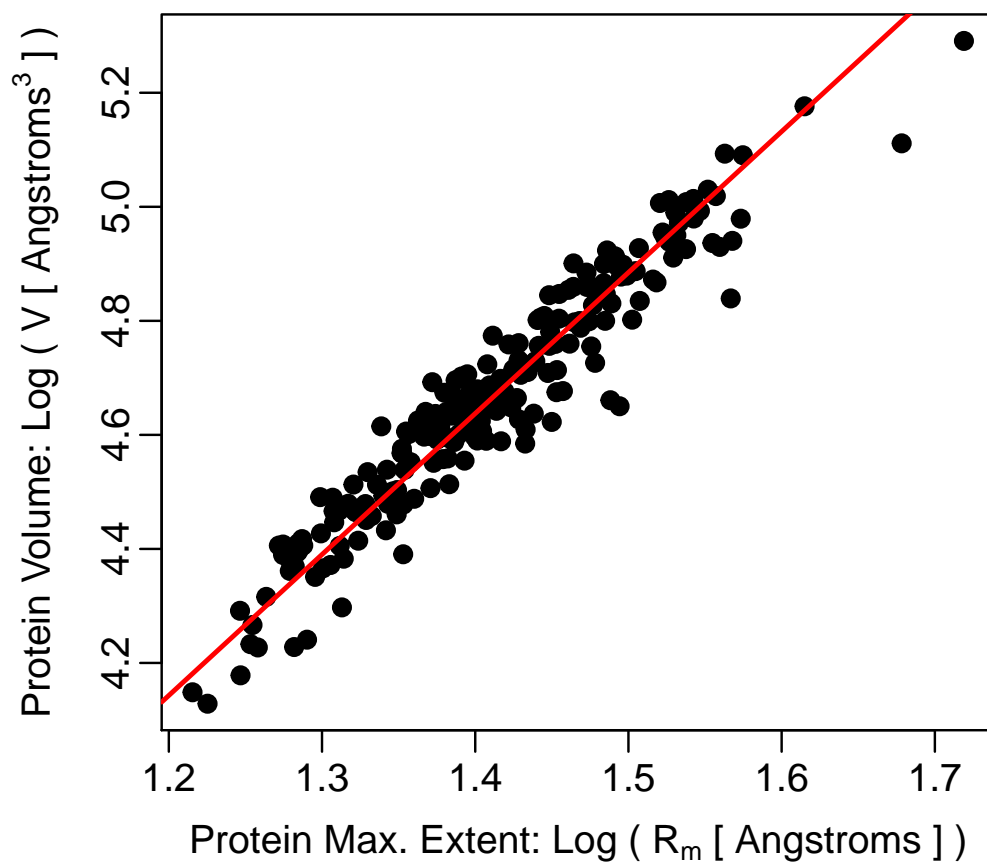


Figure 12: The scaling behavior of protein maximum extent as defined by Eqn. 13 with protein volume for 209 monomeric enzymes in the dataset. The red line is the linear Deming regression fit to logarithms of the two variables with a slope of $D \simeq 2.47 \pm 0.06$.

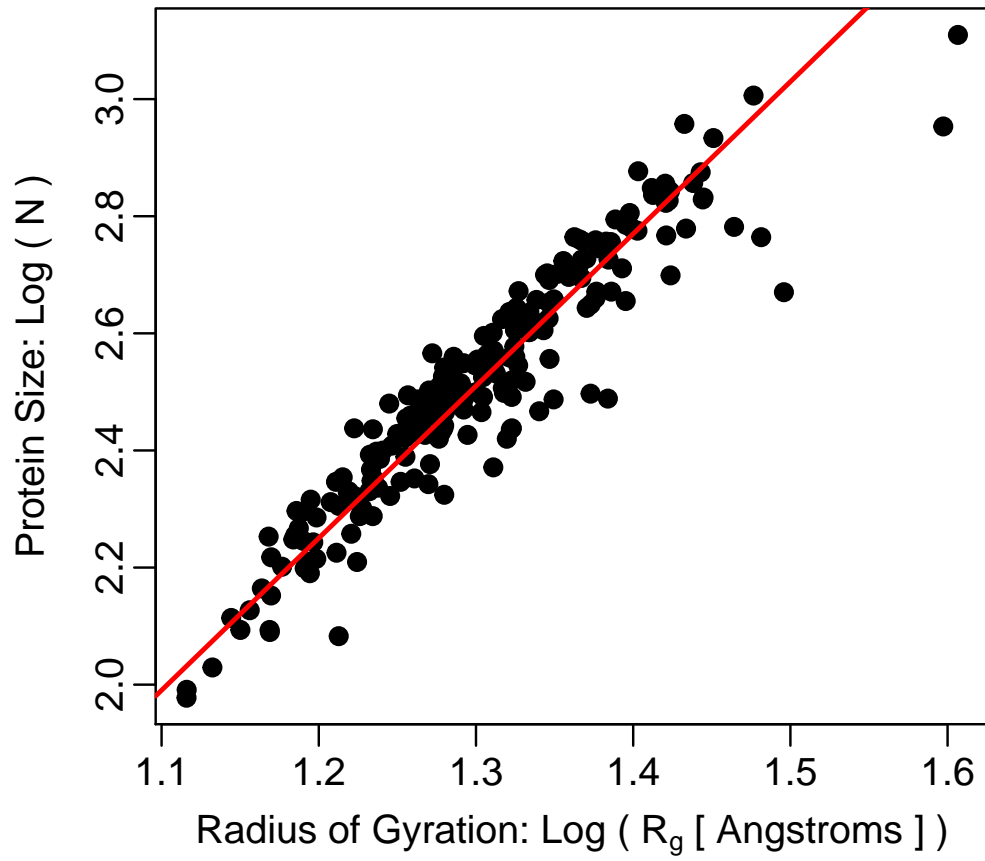


Figure 13: The scaling behavior of protein's radius as defined by Eqn. 14 with protein length for 209 monomeric enzymes in the dataset. The mean & median length of the proteins are 362 & 315 respectively. The red line is the linear Deming regression fit to logarithms of the two variables with a slope of $D \simeq 2.60 \pm 0.08$.